Analysis and Control of Modular Multilevel Converters Under Unbalanced Conditions

Yuebin Zhou, *Student Member, IEEE*, Daozhuo Jiang, Jie Guo, *Student Member, IEEE*, Pengfei Hu, and Yiqiao Liang, *Member, IEEE*

***Abstract*—This paper investigates the contents of submodule voltage ripples, circulating currents, and internal converter voltage in modular multilevel converters (MMCs) theoretically. The operation of MMCs is studied under asymmetry of the upper and lower arm, as well as the unbalanced ac system. In three-phase MMCs, the analysis shows that the second harmonic circulating currents will be asymmetric under an unbalanced ac system and can be decomposed into positive-, negative- and zero-sequence parts. The positive- and negative-sequence components affect neither the ac side nor the dc side of MMCs while the zero-sequence components will flow into the dc side, aggravating the power fluctuations of the dc side. In order to solve this problem, a new controller based on the instantaneous power theory and proportional-resonant scheme is designed. Simulations with a detailed switching model on the PSCAD/EMTDC platform verify the theoretical analysis, and demonstrate that the proposed controller eliminates the active power fluctuations and suppresses the harmonic circulating currents as well.**

***Index Terms*—Circulating current, instantaneous power theory, modular multilevel converters (MMCs), resonant frequency, stationary $\alpha\beta$ frame, submodule voltage ripple, unbalanced ac system.**

I. Introduction

MODULAR multilevel converters (MMCs) have become increasingly attractive in high-voltage (HV) applications, since they have many advantages over the traditional two-level or three-level voltage-sourced converters (VSCs) [1]–[4].

MMC was first introduced in [5]. Its structure and operation principle were studied in [1]–[4]. The pulsewidth modulation (PWM) and nearest level modulation (NLM) were investigated in [6]–[9]. It was shown in [10]–[12] that harmonic circulating currents exist in MMCs. In [13], the dynamic model of MMCs was derived. In [14], the circulating current was studied thoroughly and the resonance phenomenon existing in MMCs was verified. However, the research in [10]–[14] is under a balanced ac system. In case of an unbalanced ac system, new problems will occur and the control strategy proposed in previous research may not function properly. A back-to-back MMC-HVDC was studied in [15], where the external characteristic was focused on while the internal characteristic was not mentioned. Reference [16] developed an extended MMC-based static var compensator, but the MMC-based inverter or HVDC was not studied. In [17], a new method based on the resonant PI controller was proposed to eliminate the dc power ripple, but its design is a little complex.

Various control strategies of VSCs in case of an unbalanced ac system have been studied and the proportional resonant scheme is one of them [18]–[21], which is able to provide tracking with zero steady-state error at a certain frequency. Overall, there are mainly two control objectives about the VSCs under an unbalanced ac system. One is to keep the ac currents balanced (or suppress the negative-sequence ac current), the other is to keep the active power constant (or keep the dc voltage constant) [22]. In HVDC applications, the latter one is more important, especially in the back-to-back HVDC system.

This paper is outlined as follows. The operation principle of MMCs is introduced in Section II. Then, the SM voltage ripples, internal converter voltage, and circulating current are studied in Section III, where there is further discussion about unbalanced conditions. Finally, in Section IV, a new controller in the stationary frame is proposed, which suppresses the ac-side active power fluctuations. Meanwhile, it suppresses the dc-side power ripples by means of the cancellation of the zero-sequence second harmonic circulating current.

II. Main Circuit Configuration and Operation Principle of MMCs

For three-phase MMCs, there are six arms typically. Each arm includes N series-connected, identical half-bridge SMs, and one arm inductor L_0. In this section, a single-phase MMC is used to describe the operation principle of MMCs, as shown in Fig. 1, where the cascaded SMs per arm are represented by controllable voltage sources. The symbols are defined as follows.

R_0, L_0	equivalent arm resistance and arm inductance;
R_1, L_1	equivalent resistance and inductance at the ac side;
u_p, u_n	upper arm voltage and lower arm voltage;
i_p, i_n	arm current of the upper and lower arm;
u_s, i	ac bus voltage and ac current;
u_v	ac terminal voltage of MMCs;
e_v	internal converter voltage of MMCs;
u_{unb}	unbalanced voltage;
u_{dc}	pole-to-pole dc-bus voltage;
i_z	circulating current.

Manuscript received November 26, 2011; revised March 11, 2012, May 24, 2012, February 20, 2013, and May 06, 2013; accepted June 07, 2013. Date of publication July 02, 2013; date of current version September 19, 2013. This work was supported by the Key Innovation Team of Zhejiang Province (2010R50004), China. Paper no. TPWRD-01009-2011.

The authors are with the College of Electrical Engineering, Zhejiang University, Hangzhou 310027, Zhejiang Province, China (e-mail: zhouyuebin@zju.edu.cn; dzjiang@zju.edu.cn; guojie@zju.edu.cn).

Digital Object Identifier 10.1109/TPWRD.2013.2268981

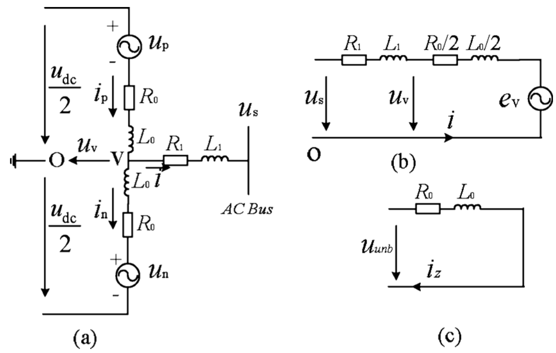

Fig. 1. Equivalent circuit of single-phase MMCs.

Subscript p and n stand for the upper and lower arm, respectively, hereinafter. According to Fig. 1(a), MMCs can be described by

$$u_s = e_v - (R_1 + 0.5R_0)i - (L_1 + 0.5L_0)di/dt \tag{1}$$
$$L_0 di_z/dt + R_0 i_z = u_{\rm unb} \tag{2}$$

where

$$e_v = (u_n - u_p)/2 \tag{3}$$
$$i_z = (i_p + i_n)/2 \tag{4}$$
$$u_{\rm unb} = u_{\rm dc}/2 - (u_n + u_p)/2. \tag{5}$$

Equations (1) and (2) represent the ac loop and the dc loop of MMCs, respectively. Fig. 1(a) and (b) is the equivalent circuit diagrams of the ac loop and the dc loop, respectively. For the sake of reduced complexity of the system model, the dc-bus voltage is considered as a constant variable, represented by $U_{\rm dc}$. It is found in (1) that e_v can be used to regulate the ac current i injected to the ac system directly, which means that the active and reactive power exchanged between the MMCs and ac system can be controlled by e_v. After considering (3) and (5), the arm voltage references can be given as

$$u_{p\_{\rm ref}} = u_{\rm dc}/2 - e_v - u_{\rm unb} \tag{6a}$$
$$u_{n\_{\rm ref}} = u_{\rm dc}/2 - e_v + u_{\rm unb}. \tag{6b}$$

By replacing (6) into (1) and (2), it is noted that $u_{\rm unb}$ in (6) has no influence on the ac loop, but the dc loop will be affected significantly, which makes it possible that $u_{\rm unb}$ can be used to improve the internal performance of MMCs, such as [10] and [12].

PWM and NLM are two basic modulation schemes applied to MMCs. The NLM is characterized for its low switching losses and convenient realization. Besides, the straightforward voltage balancing method can be implemented together with it without adding the extra controller to balance the SM voltages. Thus, in this paper, the NLM is used [9].

III. Analysis of the MMCs

A. Analysis of Single-Phase MMCs Under Balanced Condition

The internal converter voltage e_v and ac current i are given as

$$e_v = E\cos(\omega_0 t) \tag{7}$$
$$i = I\cos(\omega_0 t + \varphi) \tag{8}$$

where E and I are their amplitudes respectively; ω_0 is the fundamental frequency; φ is the power factor angle.

The arm currents of MMCs are assumed to be composed of a pure dc component and half of the ac current, shown as

$$i_p = I_{\rm dc} + i/2 \tag{9a}$$
$$i_n = I_{\rm dc} - i/2 \tag{9b}$$

where $I_{\rm dc}$ is the dc component in dc current. In the three-phase MMCs, $I_{\rm dc}$ will be one third of the total dc current at the dc side under balanced conditions. It is noting that the assumption in (9) can be achieved by applying a strategy like the CCSC in [12]. If this strategy is adopted, the arm voltage references will have the same form as (6) and in this case, the unbalance voltage is usually much smaller than $u_{\rm dc}$ [12]. Therefore, for simplified analysis below, $u_{\rm unb}$ is neglected. Modulation indexes of the upper and lower arm can be expressed as

$$F_{\rm mp} = [1 - m\cos(\omega_0 t)]/2 \tag{10a}$$
$$F_{\rm mn} = [1 + m\cos(\omega_0 t)]/2 \tag{10b}$$

where m is the modulation ratio $(0 \le m \le 1)$, defined as

$$m = 2E/U_{\rm dc}. \tag{11}$$

All of the SM voltages within one arm can be considered to be equal because of the SM voltage balancing method. Therefore, SM voltages of the upper and lower arm can be expressed as

$$u_{cp} = \frac{1}{C}\int F_{\rm mp} i_p dt \tag{12a}$$
$$u_{cn} = \frac{1}{C}\int F_{\rm mn} i_n dt \tag{12b}$$

where C is the SM capacitance. By substituting (9) and (10) into (12), the derivative of (12) is obtained shown as

$$\begin{aligned} C\frac{du_{cp}}{dt} &= F_{\rm mp} i_p \\ &= \frac{1}{2}I_{\rm dc} - \frac{1}{8}mI\cos(\varphi) - \frac{1}{8}mI\cos(2\omega_0 t + \varphi) \\ &\quad - \frac{1}{2}mI_{\rm dc}\cos(\omega_0 t) + \frac{1}{4}I\cos(\omega_0 t + \varphi) \end{aligned} \tag{13a}$$

$$\begin{aligned} C\frac{du_{cn}}{dt} &= F_{\rm mn} i_n \\ &= \frac{1}{2}I_{\rm dc} - \frac{1}{8}mI\cos(\varphi) - \frac{1}{8}mI\cos(2\omega_0 t + \varphi) \\ &\quad + \frac{1}{2}mI_{\rm dc}\cos(\omega_0 t) - \frac{1}{4}I\cos(\omega_0 t + \varphi). \end{aligned} \tag{13b}$$

In steady state, the SM voltages of MMCs should be stable. Therefore, the dc component in (13) must be zero, which means the following constraint must be satisfied:

$$I_{\rm dc} = mI\cos(\varphi)/4. \tag{14}$$

In (13), the fundamental frequency ripples between the upper arm and the lower arm have the opposite phase angle, whereas the double line-frequency ripples between them have the same phase angle. So it is reasonable to express the SM voltages as

$$u_{cp} = U_{\rm cref}[1+\varepsilon_1\cos(\omega_0 t+\varphi_1)+\varepsilon_2\cos(2\omega_0 t+\varphi_2)] \tag{15a}$$

$$u_{cn} = U_{\rm cref}[1-\varepsilon_1\cos(\omega_0 t+\varphi_1)+\varepsilon_2\cos(2\omega_0 t+\varphi_2)] \tag{15b}$$

where $U_{\rm cref}$ is the rated SM operating voltage; ε_1 and ε_2 are the ripple ranges; and φ_1 and φ_2 are the initial angles. By substituting (15) into (13), ε_1 and ε_2 can be figured out, shown as

$$\varepsilon_1 = \frac{\rm NS}{6\omega_0{\rm CU}_{\rm dc}^2}\sqrt{\frac{4}{m^2}+m^2\cos^2\varphi-4\cos^2\varphi} \tag{16}$$

$$\varepsilon_2 = \frac{\rm NS}{12\omega_0{\rm CU}_{\rm dc}^2} \tag{17}$$

where S is the apparent power, N is the SM number per arm, and $U_{\rm dc} = NU_{\rm cref}$. In (16), ε_1 is relevant to the apparent power, modulation ratio, and power factor, and it will peak at the minimum power factor.

In fact, if no measures are taken to suppress the harmonic circulating currents, the arm currents will be more complex than (9). It can be concluded from [14] that there are only even harmonic circulating currents under balanced conditions. So the circulating current can be expressed as (n is even)

$$i_z = I_{\rm dc}+\sum_{n=2}^{\infty} i_{\rm cirn} = I_{\rm dc}+\sum_{n=2}^{\infty} I_{\rm cirn}\cos(n\omega_0 t+\varphi_{\rm cirn}) \tag{18}$$

where $I_{\rm cirn}$ and $\varphi_{\rm cirn}$ are the amplitude and initial angle of the nth order harmonic. According to [14], the second harmonic in (18) is dominating. So it is reasonable to neglect the higher order ones. Then, the arm currents can be expressed as

$$i_p = I_{\rm dc}+i/2+I_{\rm cir2}\cos(2\omega_0 t+\varphi_{\rm cir2}) \tag{19a}$$

$$i_n = I_{\rm dc}-i/2+I_{\rm cir2}\cos(2\omega_0 t+\varphi_{\rm cir2}). \tag{19b}$$

According to [14], $i_{\rm cir2}$ can be calculated by

$$i_{\rm cir2} = {\rm Re}\left\{\frac{-\frac{3mI}{8\omega_0}e^{{\rm j}\varphi}+\frac{m^2 I_{\rm dc}}{2\omega_0}}{\frac{4R_0C}{N}+{\rm j}\left(\frac{8\omega_0L_0C}{N}-\frac{3+2m^2}{6\omega_0}\right)}e^{{\rm j}2\omega_0 t}\right\}. \tag{20}$$

It is interesting that a resonant point exists in (20), and the resonant frequency is

$$\omega_r = \sqrt{\frac{N(3+2m^2)}{48L_0C}}. \tag{21}$$

When $\omega_r = \omega_0, I_{\rm cir2}$ will reach its maximum value. In order to avoid the resonant point thoroughly, the maximum value of ω_r must be smaller than ω_0. Therefore, the following constraint should be satisfied:

$$L_0C > \frac{5N}{48\omega_0^2}. \tag{22}$$

The arm voltages of MMCs can be expressed as

$$u_p = {\rm NF}_{\rm mp}u_{cp} \tag{23a}$$

$$u_n = {\rm NF}_{\rm mn}u_{cn}. \tag{23b}$$

By substituting (12), (19), and (23) into (3), the internal converter voltage can be calculated, shown as

$$\begin{aligned} e_v =& \frac{1}{2}mU_{\rm dc}\cos\omega_0 t \\ &- \frac{N}{4C}\left[\frac{I}{2\omega_0}\sin(\omega_0 t+\varphi)-\frac{mI_{\rm dc}}{3\omega_0}\sin\omega_0 t\right] \\ &- \frac{mNI}{64\omega_0 C}\sin(\omega_0 t+\varphi)+\frac{3NmI_{\rm cir2}}{16\omega_0 C}\sin(\omega_0 t+\varphi_{\rm cir2}) \\ &\underbrace{-\frac{mNI}{64\omega_0 C}\sin(3\omega_0 t+\varphi)}_{e_{31}}+\underbrace{\frac{5NmI_{\rm cir2}}{48\omega_0 C}\sin(3\omega_0 t+\varphi_{\rm cir2})}_{e_{32}}. \end{aligned} \tag{24}$$

Equation (24) indicates that the 3rd harmonic in e_v is affected by the ac current (e_{31}) and the 2nd harmonic circulating current (e_{32}). However, the latter one plays a major role (seen in the Appendix). By neglecting e_{31}, the amplitude of the 3rd harmonic can be figured out approximately, shown as

$$U_3 = \frac{5mN}{48\omega_0 C}I_{\rm cir2}. \tag{25}$$

B. Analysis of Single-Phase MMCs Under Asymmetry of Upper and Lower Arms

The analysis from before is based on the fact that the ac current is split up equally between the upper and lower arm. If the upper arm and lower arm are asymmetric, such as the asymmetric arm impedance, uneven distribution of the ac current occurs. In this case, the fundamental frequency component in the arm current can be decomposed into half of the ac current and the so-called fundamental frequency circulating current. So the arm currents can be expressed as

$$\begin{aligned} i_p =& I_{\rm dc}+\frac{1}{2}i+I_{\rm cir1}\cos(\omega_0 t+\varphi_{\rm cir1}) \\ &+ I_{\rm cir2}\cos(2\omega_0 t+\varphi_{\rm cir2}) \end{aligned} \tag{26a}$$

$$\begin{aligned} i_n =& I_{\rm dc}-\frac{1}{2}i+I_{\rm cir1}\cos(\omega_0 t+\varphi_{\rm cir1}) \\ &+ I_{\rm cir2}\cos(2\omega_0 t+\varphi_{\rm cir2}) \end{aligned} \tag{26b}$$

where $I_{\rm cir1}$ and $\varphi_{\rm cir1}$ are the amplitude and initial angle of the fundamental frequency circulating current.

By substituting (26) into (13), the SM voltage ripples can be obtained. Similar to (14), the dc component must be zero, so the following equations are derived:

$$I_{\mathrm{dc}} - mI\cos\varphi/4 - mI_{\mathrm{cir1}}\cos\varphi_{\mathrm{cir1}}/2 = 0 \tag{27a}$$
$$I_{\mathrm{dc}} - mI\cos\varphi/4 + mI_{\mathrm{cir1}}\cos\varphi_{\mathrm{cir1}}/2 = 0. \tag{27b}$$

Substituting (27a) into (27b) yields

$$I_{\mathrm{cir1}}\cos\varphi_{\mathrm{cir1}} = 0. \tag{28}$$

When the upper arm and lower arm are symmetric, I_{cir1} is zero. If not, I_{cir1} will not be zero and $\cos\varphi_{\mathrm{cir1}}$ must be zero to fulfill (28). So φ_{cir1} is equal to 90° or −90°. Combining (6) and (26), the energy stored in the upper and lower arm can be expressed as

$$w_p = \int_0^t (u_{\mathrm{dc}}/2 - e_v - u_{\mathrm{unb}})i_p dt \tag{29a}$$
$$w_n = \int_0^t (u_{\mathrm{dc}}/2 + e_v - u_{\mathrm{unb}})i_n dt. \tag{29b}$$

To study the impact of fundamental frequency circulating current on the operation of MMCs, the term about e_v and the fundamental frequency circulating current are discussed. Therefore, the following equations are obtained:

$$\begin{aligned} w_{p1} &= \int_0^t -EI_{\mathrm{cir1}}\cos(\omega_0 t)\cos(\omega_0 t + \varphi_{\mathrm{cir1}})dt \\ &= -\frac{EI_{\mathrm{cir1}}}{4\omega_0}[\sin(2\omega_0 t + \varphi_{\mathrm{cir1}}) - \sin(\varphi_{\mathrm{cir1}})] \end{aligned} \tag{30a}$$
$$\begin{aligned} w_{n1} &= \int_0^t EI_{\mathrm{cir1}}\cos(\omega_0 t)\cos(\omega_0 t + \varphi_{\mathrm{cir1}})dt \\ &= \frac{EI_{\mathrm{cir1}}}{4\omega_0}[\sin(2\omega_0 t + \varphi_{\mathrm{cir1}}) - \sin(\varphi_{\mathrm{cir1}})]. \end{aligned} \tag{30b}$$

In (30), it is seen that the fundamental frequency circulating current imposes energy transfer between the upper and lower arm. However, their total energy remains unaffected. When φ_{cir1} is equal to 90°, the average energy in the upper arm is more. By contrast, when φ_{cir1} is equal to −90°, the average energy in the lower arm is more.

C. Discussion in Case of Three-Phase MMCs

The analysis of Sections III-A and B is also applicable to the three-phase MMCs, of which the dc current is nearly a pure dc component and is split up equally among the three-phase units in case of balanced conditions. According to (20), it is obvious that the 2nd harmonic circulating currents are balanced in case of balanced conditions, and in the form of negative sequence. They can be transformed to two dc components by the double-line frequency, negative-sequence rotational frame, and then suppressed by proportional-integral controllers [12]. However, under the unbalanced ac system, the second harmonic circulating currents will be unbalanced. They can be decomposed into the positive-, negative- and zero-sequence components. It should be noted that the positive- and negative-sequence components just flow among the three-phase units, without affecting the ac side and dc side, whereas the zero-sequence components will flow into the dc side, aggravating the power fluctuation at the dc side. In this case, the controller designed in [12] will not work well since it only considers the negative-sequence components. The controllers in [11] and [13] have the potential to suppress the second harmonic circulating currents under a balanced and unbalanced ac system, because they regulate the circulating current of each phase unit separately. The experimental results show good performance under balanced conditions, but no results under unbalanced conditions are presented in their works. In addition, too much computation for estimating the SM voltages is required in their controllers. Unlike [11]–[13], this paper proposes a new control scheme in the stationary frame, which works well under the balanced and unbalanced ac system.

IV. Proposed Control Strategy of MMCs

A. Control Strategy of the AC Loop

Based on the instantaneous power theory [23] and Park's transformation, the instantaneous active power delivered to the ac terminals of MMCs can be derived as

$$p_v = p_{v\mathrm{dc}} + p_{v\cos}\cos(2\omega_0 t) + p_{v\sin}\sin(2\omega_0 t) \tag{31}$$

where

$$p_{v\mathrm{dc}} = 1.5\left(u^+_{\mathrm{vd}}i^+_d + u^+_{\mathrm{vq}}i^+_q + u^-_{\mathrm{vd}}i^-_d + u^-_{\mathrm{vq}}i^-_q\right) \tag{32a}$$
$$p_{v\cos} = 1.5\left(u^+_{\mathrm{vd}}i^-_d + u^+_{\mathrm{vq}}i^-_q + u^-_{\mathrm{vd}}i^+_d + u^-_{\mathrm{vq}}i^+_q\right) \tag{32b}$$
$$p_{v\sin} = 1.5\left(u^+_{\mathrm{vd}}i^-_q - u^+_{\mathrm{vq}}i^-_d - u^-_{\mathrm{vd}}i^+_q + u^-_{\mathrm{vq}}i^+_d\right). \tag{32c}$$

The instantaneous active power and reactive power input into MMCs from the ac system are expressed as, respectively

$$p_s = p_{s\mathrm{dc}} + p_{s\cos}\cos(2\omega_0 t) + p_{s\sin}\sin(2\omega_0 t) \tag{33}$$
$$q_s = q_{s\mathrm{dc}} + q_{s\cos}\cos(2\omega_0 t) + q_{s\sin}\sin(2\omega_0 t) \tag{34}$$

where

$$p_{s\mathrm{dc}} = 1.5\left(u^+_{\mathrm{sd}}i^+_d + u^+_{\mathrm{sq}}i^+_q + u^-_{\mathrm{sd}}i^-_d + u^-_{\mathrm{sq}}i^-_q\right) \tag{35a}$$
$$p_{s\cos} = 1.5\left(u^+_{\mathrm{sd}}i^-_d + u^+_{\mathrm{sq}}i^-_q + u^-_{\mathrm{sd}}i^+_d + u^-_{\mathrm{sq}}i^+_q\right) \tag{35b}$$
$$p_{s\sin} = 1.5\left(u^+_{\mathrm{sd}}i^-_q - u^+_{\mathrm{sq}}i^-_d - u^-_{\mathrm{sd}}i^+_q + u^-_{\mathrm{sq}}i^+_d\right) \tag{35c}$$
$$q_{s\mathrm{dc}} = 1.5\left(-u^+_{\mathrm{sd}}i^+_q + u^+_{\mathrm{sq}}i^+_d - u^-_{\mathrm{sd}}i^-_q + u^-_{\mathrm{sq}}i^-_d\right) \tag{35d}$$
$$q_{s\cos} = 1.5\left(-u^+_{\mathrm{sd}}i^-_q + u^+_{\mathrm{sq}}i^-_d - u^-_{\mathrm{sd}}i^+_q + u^-_{\mathrm{sq}}i^+_d\right) \tag{35e}$$
$$q_{s\sin} = 1.5\left(u^+_{\mathrm{sd}}i^-_d + u^+_{\mathrm{sq}}i^-_q - u^-_{\mathrm{sd}}i^+_d - u^-_{\mathrm{sq}}i^+_q\right). \tag{35f}$$

In (31)–(35), $u^+_{\mathrm{vd}}, u^+_{\mathrm{vq}}, u^-_{\mathrm{vd}}$ and u^-_{vq} are the positive- and negative-sequence dq components of the ac terminal voltages. $u^+_{\mathrm{sd}}, u^+_{\mathrm{sq}}, u^-_{\mathrm{sd}}$ and u^-_{sq} are the positive- and negative-sequence dq components of the ac bus voltages. i^+_d, i^+_q, i^-_d and i^-_q are the positive- and negative-sequence dq components of the ac currents.

To keep the instantaneous active power at the ac terminals constant, the following constraint should be satisfied:

$$p_{v\mathrm{dc}} = P_{\mathrm{ref}} \tag{36a}$$
$$p_{v\cos} = p_{v\sin} = 0. \tag{36b}$$

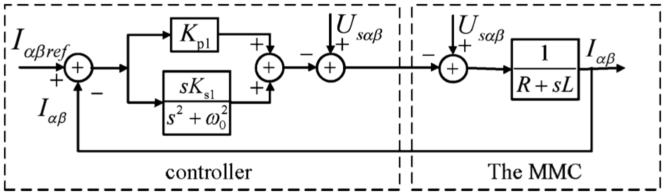

Fig. 2. Current controller of the ac loop based on the PR scheme.

Besides, another independent equation should be added to determine the reference value of i_d^+, i_q^+, i_d^- and i_q^-, shown as

$$q_{sdc} = Q_{\mathrm{ref}}. \tag{37}$$

Substituting (36) and (37) into (32) and (35d) yields

$$\begin{bmatrix} i_{d\mathrm{ref}}^+ \\ i_{q\mathrm{ref}}^+ \\ i_{d\mathrm{ref}}^- \\ i_{q\mathrm{ref}}^- \end{bmatrix} = \frac{2}{3A} \begin{bmatrix} A_{11} & A_{12} & * & * \\ A_{21} & A_{22} & * & * \\ A_{31} & A_{32} & * & * \\ A_{41} & A_{42} & * & * \end{bmatrix} \begin{bmatrix} P_{\mathrm{ref}} \\ Q_{\mathrm{ref}} \\ 0 \\ 0 \end{bmatrix} \tag{38}$$

where

$$\begin{aligned}
A &= \left(u_{\mathrm{sd}}^{-2} + u_{\mathrm{sq}}^{-2}\right)\left(u_{\mathrm{vd}}^{-2} + u_{\mathrm{vq}}^{-2}\right) \\
&\quad - \left(u_{\mathrm{sd}}^{+2} + u_{\mathrm{sq}}^{+2}\right)\left(u_{\mathrm{vd}}^{+2} + u_{\mathrm{vq}}^{+2}\right) \\
A_{11} &= -u_{\mathrm{vd}}^{-}\left(u_{\mathrm{vd}}^{+}u_{\mathrm{sd}}^{-} + u_{\mathrm{vq}}^{+}u_{\mathrm{sq}}^{-}\right) \\
&\quad - u_{\mathrm{vq}}^{-}\left(u_{\mathrm{vd}}^{+}u_{\mathrm{sq}}^{-} - u_{\mathrm{vq}}^{+}u_{\mathrm{sd}}^{-}\right) - u_{\mathrm{sd}}^{+}\left(u_{\mathrm{vd}}^{+2} + u_{\mathrm{vq}}^{+2}\right) \\
A_{21} &= -u_{\mathrm{vq}}^{-}\left(u_{\mathrm{vd}}^{+}u_{\mathrm{sd}}^{-} + u_{\mathrm{vq}}^{+}u_{\mathrm{sq}}^{-}\right) \\
&\quad + u_{\mathrm{vd}}^{-}\left(u_{\mathrm{vd}}^{+}u_{\mathrm{sq}}^{-} - u_{\mathrm{vq}}^{+}u_{\mathrm{sd}}^{-}\right) - u_{\mathrm{sq}}^{+}\left(u_{\mathrm{vd}}^{+2} + u_{\mathrm{vq}}^{+2}\right) \\
A_{31} &= u_{\mathrm{vd}}^{+}\left(u_{\mathrm{vd}}^{-}u_{\mathrm{sd}}^{+} + u_{\mathrm{vq}}^{-}u_{\mathrm{sq}}^{+}\right) \\
&\quad + u_{\mathrm{vq}}^{+}\left(u_{\mathrm{vd}}^{-}u_{\mathrm{sq}}^{+} - u_{\mathrm{vq}}^{-}u_{\mathrm{sd}}^{+}\right) + u_{\mathrm{sd}}^{-}\left(u_{\mathrm{vd}}^{-2} + u_{\mathrm{vq}}^{-2}\right) \\
A_{41} &= u_{\mathrm{vq}}^{+}\left(u_{\mathrm{vd}}^{-}u_{\mathrm{sd}}^{+} + u_{\mathrm{vq}}^{-}u_{\mathrm{sq}}^{+}\right) \\
&\quad - u_{\mathrm{vd}}^{+}\left(u_{\mathrm{vd}}^{-}u_{\mathrm{sq}}^{+} - u_{\mathrm{vq}}^{-}u_{\mathrm{sd}}^{+}\right) + u_{\mathrm{sq}}^{-}\left(u_{\mathrm{vd}}^{-2} + u_{vq}^{-2}\right) \\
A_{12} &= -u_{\mathrm{vd}}^{-}\left(u_{\mathrm{vd}}^{+}u_{\mathrm{sq}}^{-} - u_{\mathrm{vq}}^{+}u_{\mathrm{sd}}^{-}\right) \\
&\quad + u_{\mathrm{vq}}^{-}\left(u_{\mathrm{vd}}^{+}u_{\mathrm{sd}}^{-} + u_{\mathrm{vq}}^{+}u_{\mathrm{sq}}^{-}\right) - u_{\mathrm{sq}}^{+}\left(u_{\mathrm{vd}}^{+2} + u_{\mathrm{vq}}^{+2}\right) \\
A_{22} &= -u_{\mathrm{vd}}^{-}\left(u_{\mathrm{vd}}^{+}u_{\mathrm{sd}}^{-} + u_{\mathrm{vq}}^{+}u_{\mathrm{sq}}^{-}\right) \\
&\quad - u_{\mathrm{vq}}^{-}\left(u_{\mathrm{vd}}^{+}u_{\mathrm{sq}}^{-} - u_{\mathrm{vq}}^{+}u_{\mathrm{sd}}^{-}\right) + u_{\mathrm{sq}}^{+}\left(u_{\mathrm{vd}}^{+2} + u_{\mathrm{vq}}^{+2}\right) \\
A_{32} &= u_{\mathrm{vd}}^{+}\left(u_{\mathrm{vd}}^{-}u_{\mathrm{sq}}^{+} - u_{\mathrm{vq}}^{-}u_{\mathrm{sd}}^{+}\right) \\
&\quad - u_{\mathrm{vq}}^{+}\left(u_{\mathrm{vd}}^{-}u_{\mathrm{sd}}^{+} + u_{\mathrm{vq}}^{-}u_{\mathrm{sq}}^{+}\right) + u_{\mathrm{sq}}^{-}\left(u_{\mathrm{vd}}^{-2} + u_{\mathrm{vq}}^{-2}\right) \\
A_{42} &= u_{\mathrm{vd}}^{+}\left(u_{\mathrm{vd}}^{-}u_{\mathrm{sd}}^{+} + u_{\mathrm{vq}}^{-}u_{\mathrm{sq}}^{+}\right) \\
&\quad + u_{\mathrm{vq}}^{+}\left(u_{\mathrm{vd}}^{-}u_{\mathrm{sq}}^{+} - u_{\mathrm{vq}}^{-}u_{\mathrm{sd}}^{+}\right) - u_{\mathrm{sq}}^{-}\left(u_{\mathrm{vd}}^{-2} + u_{\mathrm{vq}}^{-2}\right).
\end{aligned}$$

According to (1), the mathematical model of the ac loop of a three-phase MMC in a stationary $\alpha\beta$ frame is expressed as

$$Ri_{\alpha\beta} + Ldi_{\alpha\beta}/dt = u_{s\alpha\beta} - e_{v\alpha\beta} \tag{39}$$

where

$$R = R_1 + R_0/2, \quad L = L_1 + L_0/2.$$

To control the MMCs in the stationary $\alpha\beta$ frame, a controller based on the PR scheme is designed, as shown in Fig. 2. The proposed controller regulates the overall current including the positive- and negative-sequence components. The reference values obtained by (38) must be transformed into the stationary $\alpha\beta$ frame.

According to Fig. 2, the closed-loop transfer function is

$$G_{Ic}(s) = \frac{K_{\mathrm{p1}}\left(s^2+\omega_0^2\right) + sK_{s1}}{(R+sL)(s^2+\omega_0^2) + K_{\mathrm{p1}}(s^2+\omega_0^2) + sK_{s1}}. \tag{40}$$

Substituting $s = j\omega_0$ into (40) yields

$$G_{Ic}(j\omega_0) = \frac{K_{\mathrm{p1}} * 0 + s * K_{s1}}{(R+sL)*0 + K_{\mathrm{p1}}*0 + s*K_{s1}} = 1. \tag{41}$$

Equation (41) shows that the PR scheme can realize tracking with zero steady-state error when the current reference is a sinusoidal signal with frequency ω_0.

B. Control Strategy of the DC Loop

According to the analysis in Section III-C, the circulating currents in each phase unit under the unbalanced ac system can be expressed as

$$\begin{aligned}
i_{za} &= i_{\mathrm{dc}}/3 + I_{20}\cos(2\omega_0 t + \varphi_{20}) \\
&\quad + I_{2+}\cos(2\omega_0 t + \varphi_{2+}) \\
&\quad + I_{2-}\cos(2\omega_0 t + \varphi_{2-}) && \text{(42a)} \\
i_{zb} &= i_{\mathrm{dc}}/3 + I_{20}\cos(2\omega_0 t + \varphi_{20}) \\
&\quad + I_{2+}\cos(2\omega_0 t + \varphi_{2+} - 120^\circ) + I_{2-}\cos(2\omega_0 t \\
&\quad + \varphi_{2-} + 120^\circ) && \text{(42b)} \\
i_{zc} &= i_{\mathrm{dc}}/3 + I_{20}\cos(2\omega_0 t + \varphi_{20}) \\
&\quad + I_{2+}\cos(2\omega_0 t + \varphi_{2+} + 120^\circ) \\
&\quad + I_{2-}\cos(2\omega_0 t + \varphi_{2-} - 120^\circ) && \text{(42c)}
\end{aligned}$$

where i_{dc} is the total dc current at the dc side; I_{2+}, I_{2-} and I_{20} are the amplitudes of positive-, negative- and zero-sequence circulating currents; φ_{2+}, φ_{2-}, and φ_{20} are the initial phase angles.

According to (2), the mathematical model of the dc loop of a three-phase MMC in the stationary $\alpha\beta 0$ frame is expressed as

$$R_0 i_{z\alpha\beta 0} + L_0 di_{z\alpha\beta 0}/dt = u_{unb\alpha\beta 0} \tag{43}$$

where

$$i_{z\alpha} = I_{2+}\cos(2\omega_0 t + \varphi_{2+}) + I_{2-}\cos(2\omega_0 t + \varphi_{2-}) \tag{44a}$$

$$i_{z\beta} = I_{2+}\sin(2\omega_0 t + \varphi_{2+}) + I_{2-}\sin(2\omega_0 t + \varphi_{2-}) \tag{44b}$$

$$i_{z0} = i_{\mathrm{dc}}/3 + I_{20}\cos(2\omega_0 t + \varphi_{20}). \tag{44c}$$

Similar to the control strategy of the ac loop, the control scheme of $i_{z\alpha}$ and $i_{z\beta}$ can be designed, as shown in Fig. 3. The reference value is set to zero in order to suppress the posi-

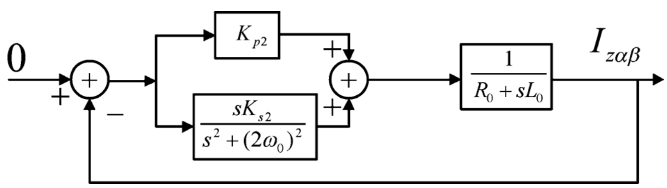

Fig. 3. Schematic diagram of $i_{z\alpha}$ and $i_{z\beta}$.

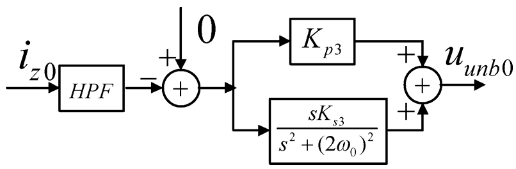

Fig. 4. Control scheme of the zero axis of the dc loop.

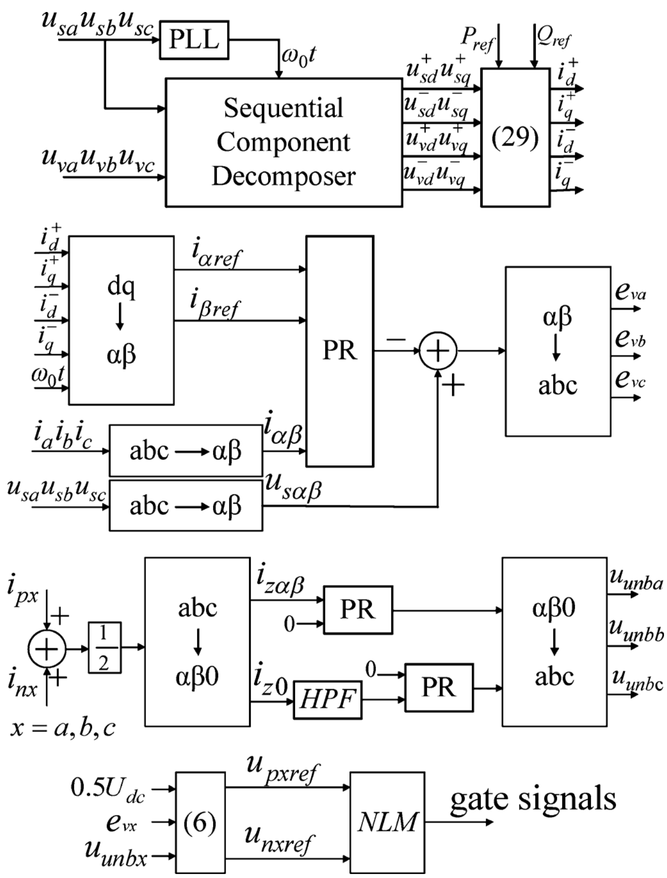

Fig. 5. Proposed overall control structure of MMCs $(x = a, b, c)$.

tive- and negative-sequence, 2nd harmonic circulating currents. Similar to (41), the PR controller in Fig. 3 can realize tracking with zero steady-state error when the current reference is a sinusoidal signal with frequency $2\omega_0$. Equation (44c) shows that i_{z0} contains the 2nd harmonic component. In order to suppress it, the controller is designed as Fig. 4, where *HPF* is the high-pass filter, whose function is to extract the fluctuation of i_{z0}.

The overall control structure is shown in Fig. 5, where the phase-locked loop (PLL) is to track the positive-sequence ac bus voltages, and the sequential component decomposer is to extract the positive- and negative- sequence components in u_{sx} and u_{vx}. NLM is the trigger module, responsible for triggering the SMs as well as balancing the SM voltages.

It should be noted that the controllers of the ac loop and dc loop are parallel. The dc-loop controller's output is much smaller than that of the ac loop. In order to suppress the second harmonic circulating currents, the total number of SMs inserted in each phase unit $(N_{\rm tx})$ may vary. According to (6), $N_{\rm tx}$ is

$$N_{\mathrm{t}x} = (U_{\mathrm{dc}} - 2u_{unbx})/U_{\mathrm{cref}}. \tag{45}$$

Since $u_{\rm unbx}$ is not zero anymore, $N_{\rm tx}$ will vary, with its maximum value larger than N. When m is very close to 1, the maximum expected number of inserted SMs in one arm may exceed the available number of SMs per arm. Therefore, there must be a few redundant SMs that exist per arm. If there are no redundant SMs or not enough, overmodulation occurs. In this paper, enough SMs are used to avoid overmodulation.

It can be inferred that the PR scheme depends on the frequency ω_0. In case it varies, the proposed controller's functionality may be affected. One solution of this problem is to add a component with a cutoff frequency to the R part [24]. This method reduces the sensitivity of the PR scheme toward frequency variation, widening the controller's bandwidth essentially, but at expense of the controller's dynamic performance. Another solution is to make the resonant frequency of the PR scheme adaptive to the frequency variation of the AC system by replacing ω_0 with the frequency obtained from PLL. In this paper, the later one is used.

V. Simulation

In order to verify the analysis in Section III and the controller proposed in Section IV, a three-phase-MMC simulation model with 80 SMs per arm is established. The model is a detailed switching model, and is built on the PSCAD/EMTDC. The main structure of the simulation model is shown in Fig. 6. Its main circuit parameters are listed in Table I.

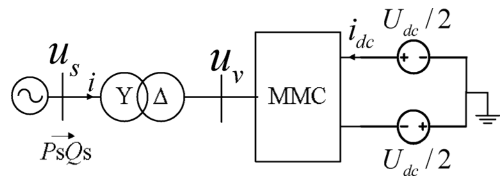

Fig. 6. Structure of the simulated model.

TABLE I
MAIN CIRCUIT PARAMETERS

Iterms	Value
Active power rating	30 MW
Rated AC system voltage (L-L, rms)	110 kV
Transformer ratio	110 kV/38 kV
Transformer leakage inductance(secondary side)	4.6 mH
Rated DC voltage	70 kV
Number of SMs per arm	80
SM capacitance	8000 uF
Arm inductance	6 mH
Rated SM operating voltage	1 kV
Equivalent arm resistance	0.8 Ω

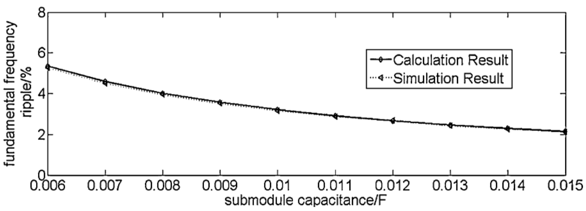

Fig. 7. Relationship between the fundamental frequency ripple and SM capacitance.

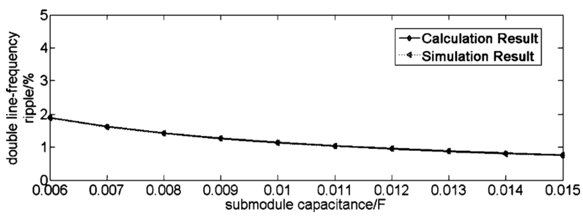

Fig. 8. Relationship between the double line-frequency ripple and SM capacitance.

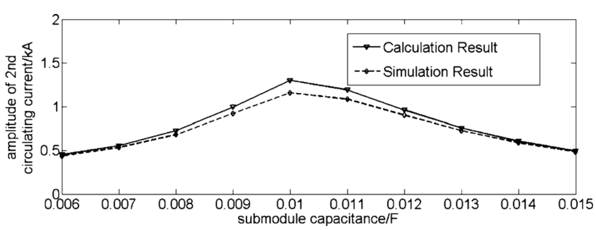

Fig. 9. . Relationship between the peak value of the second harmonic circulating current and SM capacitance.

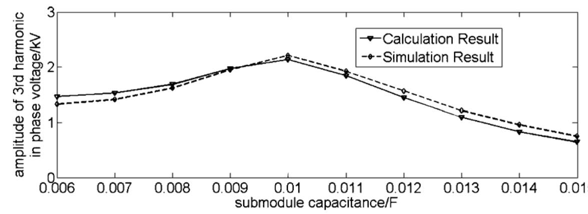

Fig. 10. . Relationship between the peak value of the third harmonic in the internal converter voltage and SM capacitance.

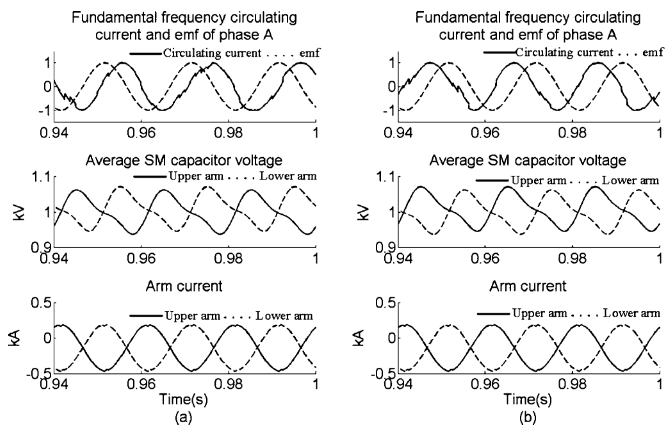

Fig. 11. Simulation results under asymmetry of the upper and lower arm. (a) Waveforms when the equivalent arm resistances of the upper and lower arms are 1.6 Ω and 0.8 Ω. (b) Waveforms when the equivalent arm resistances of the upper and lower arms are 0.8 Ω and 1.6 Ω.

Figs. 7 and 8 show the relationship between fundamental frequency, double line-frequency SM voltage ripples, and the SM capacitance, respectively, where $S = 30$ MVA and $\cos\varphi = 1$. The harmonic circulating currents are suppressed so that the arm currents only contain a dc component and half of the ac current. It is shown that the calculation results by (16) and (17) agree with the simulation results very well. This gives a proof to determine the size of SM capacitance.

Fig. 9 shows the relationship between the amplitude of the 2nd harmonic circulating current and the SM capacitance when $S = 30$ MVA and $\cos\varphi = 1$. It is found that the trends of the simulation result and the calculation result by (20) agree with each other very well. The error is mainly due to the neglect of the higher order harmonic circulating currents. This indicates that (20) can be used to calculate the 2nd harmonic circulating current approximately. The maximum amplitude of the 2nd harmonic circulating current occurs when the SM capacitance is about 0.01 F. According to (21), the SM capacitance is about 0.0105 F when the resonant frequency is equal to ω_0 ($m \approx 0.8$ in the simulation model). This demonstrates that the amplitude of the second harmonic circulating current reaches its maximum value when the resonant frequency is equal to ω_0.

Fig. 10 shows the relationship between the SM capacitance and the amplitude of the 3rd harmonic in the internal converter voltage. The simulation result and the calculation result agree with each other very well. This demonstrates that (25) can generally describe the relationship between the third harmonic in the internal converter voltage and the second harmonic circulating current.

Fig. 11 shows the simulation results with asymmetric arm impedance between the upper and lower arm. The upper chart shows the generalized waveforms of the fundamental frequency circulating current and the internal converter voltage (emf) of phase A. When the waveform of the fundamental frequency circulating current lags 90° than that of the emf [Fig. 11(a)], the average SM voltage of the lower arm is larger. When the waveform of the fundamental frequency circulating current leads 90° than that of the emf [Fig. 11(b)], the average SM voltage of the upper arm is larger.

In order to verify the control scheme proposed in Section IV, three cases are studied.

1) Active/Reactive Power Control Under Balanced AC System Operation: Initially, the active power and reactive power are set to 0. The active power is step changed at $\mathrm{t} = 0.4$ s, from 0 to -30 MW. The reactive power is step changed at $\mathrm{t} = 0.5$ s, from 0 to $-$ 10 Mvar. Then, at $\mathrm{t} = 0.6$ s, the active power flow reversal occurs from -30 to 30 MW within 12.5 ms. The simulation results are shown in Fig. 12.

The active power and reactive power are shown in Fig. 12(a). It can be seen that $p_{v\,\sin}$ and $p_{v\,\cos}$ are almost zero during steady state. Meanwhile, the active power $p_{v\mathrm{dc}}$ and the reactive power $q_{s\mathrm{dc}}$ are regulated to their reference value. This indicates that the active power exchanged between the ac side and dc side is generally constant. In Fig. 12(b) and (c), there are no noticeable changes in the output voltages (the ac terminal voltages), whereas the output currents are affected more or less during the

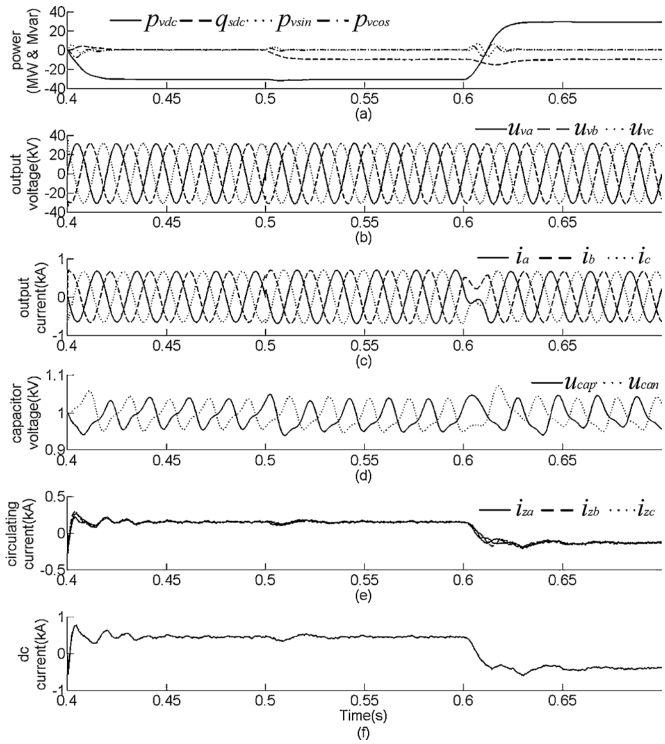

Fig. 12. Simulation results under the balanced ac system. (a) Active and reactive power at the ac terminal. (b) Output voltages. (c) Output currents. (d) Average SM voltages in upper and lower arms of phase A. (e) Circulating currents. (f) DC current.

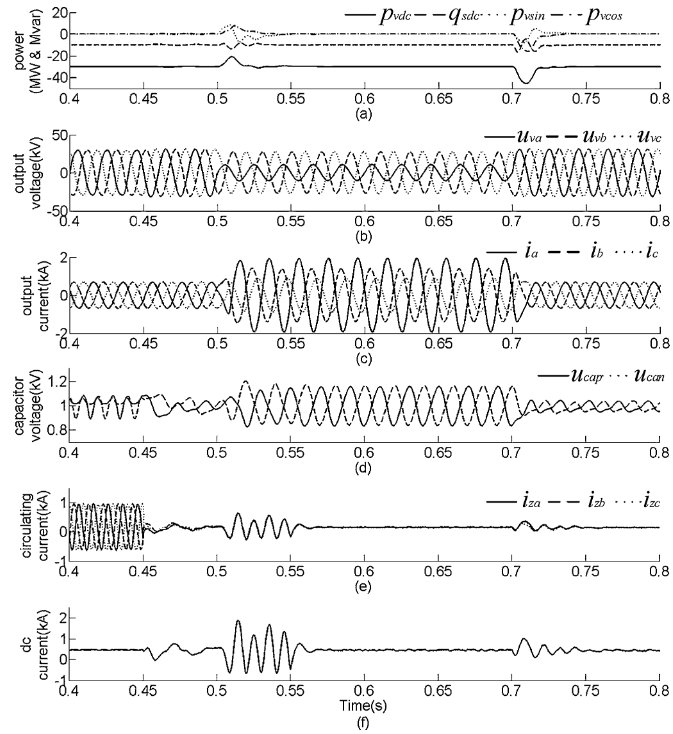

Fig. 13. Simulation results under the unbalanced ac system. (a) Active and reactive power at the ac terminal. (b) Output voltages. (c) Output currents. (d) Average SM voltages in the upper and lower arms of phase A. (e) Circulating currents. (f) DC current.

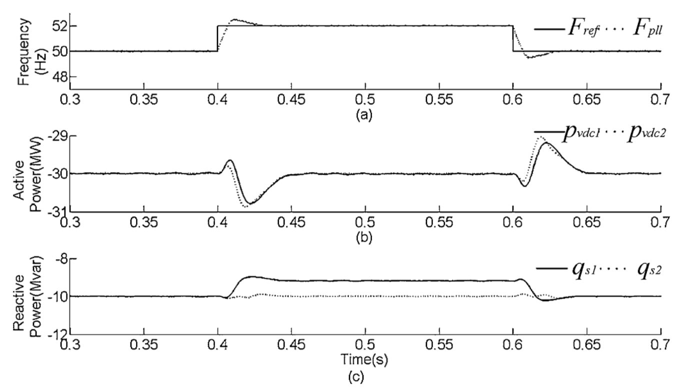

Fig. 14. Active power and reactive power flow in case of frequency variation. (a) Response of the PLL to frequency's step change. (b) Active power. (c) Reactive power.

transients. Fig. 12(d) shows that the average SM voltages of the upper and lower arms of phase A vary within 5% of the ratings. The 2nd harmonic circulating current is suppressed very well during the transients and steady state, as shown in Fig. 12(e).

2) Single-Phase-to-Ground Fault Operation: The MMC operates at -30 MW active power and -10 Mvar reactive power. The controller in Fig. 3 is enabled at t $= 0.45$ s. The phase A to ground fault is imposed at t $= 0.5$ s, lasting for 0.2 s. The controller in Fig. 4 is enabled at t $= 0.55$ s. The simulation results are shown in Fig. 13.

It is shown in Fig. 13(a) that $p_{v\,\sin}$ and $p_{v\,\cos}$ are almost zero during the normal and fault period. Meanwhile, the active power $p_{v\mathrm{dc}}$ and the reactive power $q_{s\mathrm{dc}}$ are regulated to their reference value. The output voltages and output currents are observed in Fig. 13(b) and (c). For the sake of keeping the instantaneous active power at the ac side constant, the output voltages and output currents become unbalanced during the fault period. Fig. 13(d) shows the SM voltages of phase unit A. The circulating currents and dc current are shown in Fig. 13(e) and (f), respectively.

It is seen that before $t = 0.45$ s, the second harmonic circulating currents are significant. However, the dc current is nearly a pure dc component. Meanwhile, the SM voltage ripples are complex. The second harmonic circulating currents are quickly suppressed to a low level with the controller in Fig. 3 enabled at $t = 0.45$ s. The amplitude of the SM voltage ripples also becomes smaller. At $t = 0.5$ s, the phase-A-to-ground fault is imposed. The second harmonic, zero-sequence circulating currents appear, which makes the dc current also contain fluctuations with double line-frequency, aggravating the power fluctuation at the dc side. At $t = 0.55$ s, the controller designed in Fig. 4 is enabled, and it quickly works. The fluctuation in dc current is suppressed significantly.

3) Response to Frequency Variation of AC System Operation: The MMC operates at -30-MW active power and -10-Mvar reactive power. The frequency of the ac system is step changed at $t = 0.4$ s from 50 to 52 Hz, and back to 50 Hz at $t = 0.6$ s. Two contrary simulations are made to investigate the influence of frequency variation on the PR scheme. One is to keep the resonant frequency constant, equal to 50 Hz. The other one is to keep the resonant frequency adaptive to the frequency obtained from PLL. The simulation results are shown in Fig. 14.

Fig. 14(a) shows the response of the PLL to the frequency's step change, where F_{ref} is the reference value and F_{pll} is the

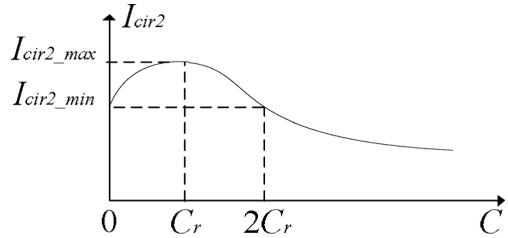

Fig. 15. Typical relationship between the SM capacitance and I_{cir2}.

output of the PLL. In Fig. 14(b) and (c), the active power and reactive power are shown, where $p_{v\mathrm{dc1}}$ and q_{s1} have constant frequency whereas $p_{v\mathrm{dc2}}$ and q_{s2} have variable frequency. It is seen that with the constant frequency, the PR scheme commits a steady-state error when the frequency of the ac system deviates from 50 Hz. However, it works well if the resonant frequency is replaced by the PLL's output frequency.

VI. Conclusion

The fundamental frequency component of the SM voltage peaks at the minimum power factor, whereas the double line-frequency component is only related to the apparent power. Therefore, the SM capacitance should be determined when MMCs operate with full power and minimum power factor.

The fundamental frequency circulating current causes energy transfer between the upper and lower arm. The second harmonic circulating current peaks when *LC* resonance occurs. The third harmonic in the internal converter voltage is closely related to the second harmonic circulating current.

The harmonic circulating currents increase the arm current rms and aggravate the SM voltage ripples. A large L_0 is helpful to suppress the harmonic circulating currents, but this is costly. The CCSC can help to suppress the harmonic circulating currents, and decrease the size of the arm inductance. In case of the unbalanced ac system, the second harmonic, zero-sequence circulating currents flow into the dc side, aggravating the power fluctuation of the dc side. The proposed controller works well under a balanced and unbalanced ac system, even if the frequency of the ac system varies.

Appendix

It is reasonable to neglect the equivalent arm resistance when the resonant frequency in (21) is far away from ω_0. Therefore, by substituting (14) into (21), I_{cir2} can be approximately obtained as

$$I_{\mathrm{cir2}} \approx \frac{mI}{8\omega_0} \frac{\|(m^2-3)\cos\varphi - \mathrm{j}3\sin\varphi\|}{\left|\frac{8\omega_0 L_0 C}{N} - \frac{3+2m^2}{6\omega_0}\right|}. \tag{46}$$

With the SM capacitance varying from zero to infinity, I_{cir2} will increase to its maximum value $I_{\mathrm{cir2\_max}}$ first and then decrease to zero gradually. The typical relationship between C and I_{cir2} is shown in Fig. 15, with a fixed m. When $C = C_r$, I_{cir2} will reach its maximum value. A large L_0 leads to a small C_r, and is helpful to avoid the resonant phenomenon, and to lower I_{cir2}, but it is costly. In this paper, a reasonable L_0 is used to make C_r large enough. Only the interval $(0, 2C_r]$ is discussed. Therefore, the minimum value of I_{cir2} can be calculated by

$$I_{\mathrm{cir2\_min}} \approx \frac{3mI}{4} \frac{\|(m^2-3)\cos\varphi - \mathrm{j}3\sin\varphi\|}{3+2m^2} = KI \tag{47}$$

where

$$K = \frac{3m}{4} \frac{\|(m^2-3)\cos\varphi - \mathrm{j}3\sin\varphi\|}{3+2m^2}. \tag{48}$$

By substituting (47) into (24), the 3rd harmonic of e_v is

$$e_3 = \frac{5mNKI}{48\omega_0 C}\sin(3\omega_0 t + \varphi_{\mathrm{cir2}}) - \frac{mNI}{64\omega_0 C}\sin(3\omega_0 t + \varphi). \tag{49}$$

Normally, m is close to 1. Therefore, K can be calculated approximately as

$$K = 3\sqrt{4 + 5\sin^2\varphi}/20 \in [0.3, 0.45]. \tag{50}$$

By substituting (50) into (49), the amplitude of the first term in (49) will be larger than that of the second term. If the resonant frequency is around ω_0, the first term will be dominating.

References

[1] R. Marquardt, "Modular multilevel converter: An universal concept for HVDC-networks and extended DC-bus-applications," in *Proc. Power Electron. Int. Conf.*, Jun. 21–24, 2010, pp. 502–507.

[2] A. Lesnicar and R. Marquardt, "An innovative modular multilevel converter topology suitable for a wide power range," presented at the IEEE Bologna Power Tech Conf., Bologna, Italy, Jun. 23–26, 2003.

[3] J. Dorn, H. Huang, and D. Retzmann, "Novel voltage-sourced converters for HVDC and FACTS applications," presented at the CIGRE Symp., Osaka, Japan, 2007.

[4] J. Dorn, H. Huang, and D. Retzmann, "A new multilevel voltage sourced converter topology for HVDC applications," in *Proc. CIGRE*, Paris, France, 2008, pp. 1–8, paper B4-304.

[5] R. Marquardt, "Stromrichterschaltungen Mit Verteilten- Energiespeichern," German Patent DE10103031A1, Jan. 24, 2001.

[6] M. Hagiwara and H. Akagi, "Control and experiment of pulsewidth-modulated modular multilevel converters," *IEEE Trans. Power Electron.*, vol. 24, no. 7, pp. 1737–1746, Jul. 2009.

[7] S. Rohner, S. Bernet, M. Hiller, and R. Sommer, "Pulse width modulation scheme for the modular multilevel converter," in *Proc. 13th Eur. Conf. Power Electron. Appl.*, Sep. 8–10, 2009, pp. 1–10.

[8] A. Das, H. Nademi, and L. Norum, "A pulse width modulation technique for reducing switching frequency for modular multilevel converter," in *Proc. India Int. Conf. Power Electron.*, Jan. 28–30, 2011, pp. 1–6.

[9] Q. Tu and Z. Xu, "Impact of sampling frequency on harmonic distortion for modular multilevel converter," *IEEE Trans. Power Del.*, vol. 26, no. 1, pp. 298–306, Jan. 2011.

[10] A. Antonopoulos, L. Angquist, and H. P. Nee, "On dynamics and voltage control of the modular multilevel converter," in *Proc. 13th Eur. Conf. Power Electron. Appl.*, Sep. 8–10, 2009, pp. 1–10.

[11] L. Angquist, A. Antonopoulos, D. Siemaszko, K. Ilves, M. Vasiladiotis, and H. P. Nee, "Inner control of modular multilevel converters—An approach using open-loop estimation of stored energy," in *Proc. Int. Power Electron. Conf.*, Jun. 21–24, 2010, pp. 1579–1585.

[12] Q. Tu, Z. Xu, and L. Xu, "Reduced switching-frequency modulation and circulating current suppression for modular multilevel converters," *IEEE Trans. Power Del.*, vol. 26, no. 3, pp. 2009–2017, Jul. 2011.

[13] L. Harnefors, S. Norrga, A. Antonopoulos, and H. P. Nee, "Dynamic modeling of modular multilevel converters," in *Proc. 14th Eur. Conf. Power Electron. Appl.*, Aug. 30–Sep. 1 2011, pp. 1–10.

[14] K. Ilves *et al.*, “Steady-state analysis of interaction between harmonic components of arm and line quantities of modular multilevel converters,” *IEEE Trans. Power Electron.*, vol. 27, no. 1, pp. 57–68, Jan. 2011.
[15] M. Saeedifard and R. Iravani, “Dynamic performance of a modular multilevel back-to-back HVDC system,” *IEEE Trans. Power Del.*, vol. 25, no. 4, pp. 2903–2912, Oct. 2010.
[16] H. M. Pirouz and M. T. Bina, “New transformerless medium-voltage STATCOM based on half-bridge cascaded converters,” in *Proc. 1st Power Electron. Drive Syst. Technol. Conf.*, Feb. 17–18, 2010, pp. 129–134.
[17] G. Bergna, J. Suul, and E. Berne, “Mitigating DC-side power oscillations and negative sequence load currents in modular multilevel converters under unbalanced faults—First approach using resonant PI,” in *Proc. IEEE 38th Annu. Conf. Ind. Electron. Soc.*, Oct. 25–28, 2012, pp. 537–542.
[18] X. Yuan, J. Allmeling, W. Merk, and H. Stemmler, “Stationary frame generalized integrators for current control of active power filters with zero steady state error for current harmonics of concern under unbalanced and distorted operation conditions,” in *Proc. IEEE Ind. Appl. Conf.*, Oct. 2000, vol. 4, pp. 2143–2150.
[19] Y. Sato, T. Ishizuka, K. Nezu, and T. Kataoka, “A new control strategy for voltage-type PWM rectifiers to realize zero steady-state control error in input current,” *IEEE Trans. Ind. Appl.*, vol. 34, no. 3, pp. 480–486, May/Jun. 1998.
[20] J. Hu and Y. He, “Modeling and control of grid-connected voltage-sourced converters under generalized unbalanced operation conditions,” *IEEE Trans. Energy Convers.*, vol. 23, no. 3, pp. 903–913, Sep. 2008.
[21] A. Timbus, M. Liserre, R. Teodorescu, P. Rodriguez, and F. Blaabjerg, “Evaluation of current controllers for distributed power generation systems,” *IEEE Trans. Power Electron.*, vol. 24, no. 3, pp. 654–664, Mar. 2009.
[22] A. Yazdani and R. Iravani, “A unified dynamic model and control for the voltage-sourced converter under unbalanced grid conditions,” *IEEE Trans. Power Del.*, vol. 21, no. 3, pp. 1620–1629, Jul. 2006.
[23] H. Akagi, Y. Kanazawa, and A. Nabae, “Instantaneous reactive power compensation comprising switching devices without energy storage components,” *IEEE Trans. Ind. Appl.*, vol. IA-20, no. 3, pp. 625–630, May/Jun. 1984.
[24] J. Hu, Y. He, L. Xu, and B. W. Williams, “Improved control of DFIG systems during network unbalance using PI-R current regulators,” *IEEE Trans. Ind. Electron.*, vol. 56, no. 2, pp. 439–451, Feb. 2009.

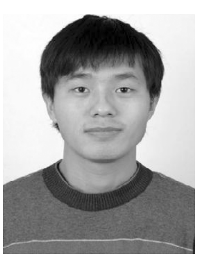

Yuebin Zhou (S’12) was born on February 15, 1987, in Shaanxi, China. He received the B.E. degree in electrical engineering from Zhejiang University, Hangzhou, China, in 2009, where he is currently pursuing the Ph.D. degree in electrical engineering.

His research interests include high-voltage dc transmission and flexible ac transmission systems.

Daozhuo Jiang was born on July 21, 1960, in Minhou, China.

Currently, he is a Professor with the College of Electrical Engineering, Zhejiang University. His research fields include control technologies for alternating and direct current power systems, power electronic and flexible ac transmission systems, smart measurement and control technologies, and distribution network automation.

Jie Guo (S’10) was born in Baoding, China, on December 4, 1985. He received the B.E. degree in power system and its automation from North China Electric Power University, Baoding, China, in 2008 and is currently pursuing the Ph.D. degree in electrical engineering at Zhejiang University, Hangzhou, China.

His research interests include high-voltage dc transmission and flexible ac transmission systems.

Pengfei Hu was born in Suining, China, on January 8, 1988. He received the B.E. degree in electrical engineering and its automation from the College of Electrical Engineering, Zhejiang University, Hangzhou, China, in 2010, where he is currently pursuing the Ph.D. degree in electrical engineering.

His research interests include high-voltage dc transmission and flexible ac transmission systems.

Yiqiao Liang (M’98) received the B.S. and M.S. degrees in electrical engineering from Zhejiang University, Hangzhou, China, in 1984 and 1987, respectively, and the Ph.D. degree in electrical engineering from Drexel University, Philadelphia, PA, in 2000.

Currently, he is a Research Fellow with the College of Electrical Engineering, Zhejiang University. His research interests are in the fields of power electronics and power systems.